



Article

Anisotropic Growth and Magnetic Properties of α'' -Fe₁₆N₂@C Nanocones

Yong Li ¹, Qifeng Kuang ¹, Xiaoling Men ¹, Shenggang Wang ¹ , Da Li ^{1,*} , Chuljin Choi ^{2,*} and Zhidong Zhang ¹

¹ Shenyang National Laboratory for Materials Science, Institute of Metal Research, Chinese Academy of Sciences, 72 Wenhua Road, Shenyang 110016, China; yli14s@163.com (Y.L.); qfkuang18b@imr.ac.cn (Q.K.); xlm19b@imr.ac.cn (X.M.); sgwang@imr.ac.cn (S.W.); zdzhang@imr.ac.cn (Z.Z.)

² Korea Institute of Materials Science, 797 Changwondaero, Seongsangu, Changwon 51508, Gyeongnam, Korea

* Correspondence: dali@imr.ac.cn (D.L.); cjchoi@kims.re.kr (C.C.);
Tel.: +86-24-83978846 (D.L.); +82-55-280-3532 (C.C.)

Abstract: α'' -Fe₁₆N₂ nanomaterials with a shape anisotropy for high coercivity performance are of interest in potential applications such as rare-earth-free permanent magnets, which are difficult to synthesize in situ anisotropic growth. Here, we develop a new and facile one-pot microemulsion method with Fe(CO)₅ as the iron source and tetraethylenepentamine (TEPA) as the N/C source at low synthesis temperatures to fabricate carbon-coated tetragonal α'' -Fe₁₆N₂ nanocones. Magnetocrystalline anisotropy energy is suggested as the driving force for the anisotropic growth of α'' -Fe₁₆N₂@C nanocones because the easy magnetization direction of tetragonal α'' -Fe₁₆N₂ nanocrystals is along the c axis. The α'' -Fe₁₆N₂@C nanocones agglomerate to form a fan-like microstructure, in which the thin ends of nanocones direct to its center, due to the magnetostatic energy. The lengths of α'' -Fe₁₆N₂@C nanocones are ~200 nm and the diameters vary from ~10 nm on one end to ~40 nm on the other end. Carbon shells with a thickness of 2–3 nm protect α'' -Fe₁₆N₂ nanocones from oxidation in air atmosphere. The α'' -Fe₁₆N₂@C nanocones synthesized at 433 K show a room-temperature saturation magnetization of 82.6 emu/g and a coercive force of 320 Oe.

Keywords: α'' -Fe₁₆N₂; permanent magnetic material; one-dimensional nanocones; core/shell structure; anisotropic growth; chemical solution method



Citation: Li, Y.; Kuang, Q.; Men, X.; Wang, S.; Li, D.; Choi, C.; Zhang, Z. Anisotropic Growth and Magnetic Properties of α'' -Fe₁₆N₂@C Nanocones. *Nanomaterials* **2021**, *11*, 890. <https://doi.org/10.3390/nano11040890>

Academic Editor:
Alberto López-Ortega

Received: 18 February 2021
Accepted: 27 March 2021
Published: 31 March 2021

Publisher's Note: MDPI stays neutral with regard to jurisdictional claims in published maps and institutional affiliations.



Copyright: © 2021 by the authors. Licensee MDPI, Basel, Switzerland. This article is an open access article distributed under the terms and conditions of the Creative Commons Attribution (CC BY) license (<https://creativecommons.org/licenses/by/4.0/>).

1. Introduction

Permanent magnets can provide a high efficiency and reliability for renewable energy technologies, such as wind turbines and hybrid electric vehicles [1]. Rare-earth-free permanent magnets, expected to be the next generation of permanent magnetic materials, have been paid much attention due to abundant resources, low cost, large coercivity and high Curie temperatures [2]. Body-centered tetragonal (bct) α'' -Fe₁₆N₂, being an ordered nitride, is one of the most promising candidates for future applications of rare-earth-free permanent magnets because of the excellent magnetocrystalline anisotropy (7.8×10^5 J/m³) and the highest saturation magnetization reported so far [3–8]. In the iron–nitrogen binary system, Jack first reported that the metastable phase α'' -Fe₁₆N₂ has a giant magnetic moment [9]. Besides α'' -Fe₁₆N₂, ferromagnetic iron nitrides include a hexagonal close packed ϵ -phase with general formula ϵ -Fe₃N_{1+x} showing a wide range of composition range with extreme values of $-0.40 < x < 0.48$, and the face-centered cubic γ' -Fe₄N. Face-centered cubic γ' -Fe₄N has a ferromagnetic state below its Curie temperature of about 760 K [10], while ϵ -Fe₃N ($x \leq 0$) in a space group P6₃22 with all the N atoms occupying octahedral interstices (2c site) exhibits a well-ordered structure, showing enhancements of the Curie temperature (T_C) and room-temperature saturation magnetization (M_S) with decreasing N content, with a record-high T_C (632 K) and M_S (192 emu/g) at $x = 0.88$ [11]. The magnetic moment of iron atoms on the 4d site of α'' -Fe₁₆N₂ is 3.0 μ_B /Fe [12]. The M_S of partially

ordered Fe_{16}N_2 thin films increases monotonically with an increasing volume ratio of the $\alpha''\text{-Fe}_{16}\text{N}_2$ and the N site ordering parameter related on the special arrangement of Fe_6N clusters [13]. Anisotropic $\alpha''\text{-Fe}_{16}\text{N}_2$ magnets were prepared by starting from pure bulk Fe with urea as the nitrogen source [14]. Because of optimal coercivity performance of single-domain nanoparticles, the lower dimensionality of the enhanced hard magnetic properties of magnetic nanostructures has been attractive in the area of hard magnetic nanomaterials [2,15,16]. Well-controlled nanostructures of hard magnets are a possible future choice for controlling texture and magnetic alignment to support high-density magnetic storage and giant energy density [17].

$\alpha''\text{-Fe}_{16}\text{N}_2$ powders and nanoparticles were obtained by mechanical ball milling with a solid nitrogen source of NH_4NO_3 [18] and ammonia nitrification of iron nanoparticles after being reduced from Fe-oxide nanoparticles [19], showing a coercivity (H_C) as high as 3.35 kOe. Core-shell $\alpha''\text{-Fe}_{16}\text{N}_2/\text{SiO}_2$ [20], $\alpha''\text{-Fe}_{16}\text{N}_2/\text{C}$ [21] and $\alpha''\text{-Fe}_{16}\text{N}_2/\text{Al}_2\text{O}_3$ nanoparticles [22] were obtained through various successive procedures starting from the reduction of Fe-oxides, followed by nitridation. The core-shell structure can restrict the growth of $\alpha''\text{-Fe}_{16}\text{N}_2$ nanoparticles during the nitridation process, which improves the coercivity performance of $\alpha''\text{-Fe}_{16}\text{N}_2$ nanoparticles. However, the M_S values experimentally determined in $\alpha''\text{-Fe}_{16}\text{N}_2$ nanoparticles were in the range 160–225 emu/g, smaller than the value (290 emu/g) for $\alpha''\text{-Fe}_{16}\text{N}_2$ thin film [9,13,23,24]. In nanowire arrays, the dipole–dipole interaction between wires becomes important [25]. By combination of the shape anisotropy and the magneto-crystalline anisotropy, ferromagnetic materials with a high magnetic anisotropy exhibit a high coercivity [15].

The most common synthesis route for iron nitrides is nitridation of iron films, powders and nanoparticles in an NH_3 atmosphere at high temperatures (≥ 573 K) [26–29]. Such high-temperature nitridation routes inevitably create disordered nitrogen atoms in iron nitrides. The chemical solution method is mild and highly effective to synthesize high-purity magnetic nanocrystals with controlled composition, size and microstructure by varying the reaction conditions [16,30]. Recently, nanoscale and stable $\varepsilon\text{-Fe}_3\text{N}_{1+x}$ ($-0.12 \leq x \leq -0.01$) nanoparticles with highly ordered N atoms were obtained by using iron(II) acetylacetonate and tetraethylenepentamine (TEPA) as Fe and N/C sources under a lower temperature (533 K) [11]. Such a novel chemical synthesis route is favorable for preparation of monophasic $\varepsilon\text{-Fe}_3\text{N}_{1+x}$ ($x < 0$) nanoparticles that were never synthesized previously because the $\varepsilon\text{-Fe}_3\text{N}_{1+x}$ ($x < 0$) phases are unstable at a temperature lower than their synthesis temperatures [31,32]. Due to thermal instability at ~ 523 K, the synthesis of $\alpha''\text{-Fe}_{16}\text{N}_2$ with highly ordered N atom occupancies is usually at a nitridation temperature lower than 453 K [33–35]. Improvements thereof are expected in the chemical synthesis for $\alpha''\text{-Fe}_{16}\text{N}_2$ and its magnetic properties. Herein, carbon-coated one-dimensional (1D) $\alpha''\text{-Fe}_{16}\text{N}_2$ nanocones with an average length of 200 nm were synthesized by a new simple low-temperature chemical solution method. Anisotropic growth mechanism, structure and magnetic performance of the $\alpha''\text{-Fe}_{16}\text{N}_2@\text{C}$ nanocones were studied.

2. Materials and Methods

2.1. Chemicals

Iron pentacarbonyl [$\text{Fe}(\text{CO})_5$, 98%], 1-octadecene (ODE, 90%) and oleylamine (OLA, 90%) were purchased from Aladdin reagent company (Shanghai, China). Absolute ethanol (99.7%) and tetraethylenepentamine (TEPA, 90%) were purchased from Sinopharm Chemical Reagent Co. Ltd. (Shenyang, China). Prior to synthesis, the original TEPA was heated to 588 K in a nitrogen atmosphere and kept at this temperature for 5 h. Other chemicals were used without further purification.

2.2. Synthesis of $\alpha''\text{-Fe}_{16}\text{N}_2@\text{C}$ Nanocones

The solution syntheses were carried out at a reaction temperature range from 393 to 553 K with a varied reaction time of 1 and 6 days. When the reaction temperature and reaction time were less than 433 K and 3 days, both Fe_3O_4 and $\alpha\text{-Fe}$ were usually found in

the products because the nitridation reactions were incomplete. In a typical synthesis of α'' -Fe₁₆N₂@C nanocones, 10 mL of the treated TEPA, 30 mL of ODE and 10 mL of OLA were mixed into a 250 mL four-neck flask using a Schlenk line under air-free conditions and magnetically stirred throughout the entire reaction process. Under a mixed Ar/H₂ (95:5) flow, the mixture was first heated to 383 K. The solution was kept at this temperature for 60 min. to remove low boiling-point solvent and oxygen. Then, the temperature was increased to 473 K at 5 K·min⁻¹ and a translucent yellow microemulsion was obtained. At 473 K, a mixed solution consisted of 2 mL of Fe(CO)₅, 6 mL of ODE and 2 mL of OLA in a syringe which was injected into the microemulsion at a rate of 30 mL/h and maintained at this temperature for 30 min. for the formation of Fe nanocrystals (NCs). Subsequently, the reaction system was cooled to 433 K and maintained at this temperature for 6 days, at which temperature α'' -Fe₁₆N₂ was synthesized. At room temperature, the product was precipitated by centrifugation at 3000 × g rpm for 5 min. The precipitate was rewashed in 20 mL of ethanol three times and dried in a vacuum for further characterization.

2.3. Characterization

The size, morphology and microstructure of the α'' -Fe₁₆N₂@C nanocones were observed using a Tecnai G2 F20 transmission electron microscope (TEM) (FEI Inc., Hillsboro, OR, USA) at 200 kV. The scanning electron microscopy (SEM) images were obtained with a JSM 6301F field-emission scanning electron microscope (FESEM) system (JEOL Inc., Tokyo, Japan). Powder X-ray diffraction (XRD) was recorded on a D/Max-2400 diffractometer (Rigaku Inc., Tokyo, Japan) equipped with a Cu K_α radiation source ($\lambda = 0.154056$ nm). The composition and surface information of the nanocones were determined by X-ray photoelectron spectroscopy (XPS) (Thermo Fisher Inc., Waltham, MA, USA). The surface of compacted samples was cleaned by argon-ion bombardment. Both the as-prepared and the surface-cleaned samples were analyzed by the XPS to determine the species covering on the surface of samples. Thermal analysis was performed on an STA6000 thermal analyzer (PerkinElmer Inc., Waltham, MA, USA) under N₂ flow with heating rate of 10 K·min⁻¹ between 300 and 900 K. Room-temperature magnetic hysteresis loop and temperature-dependent magnetization in the rising/cooling processes (at $H = 1$ kOe) were carried out using a vibrating sample magnetometer (VSM) in a physical property measurement system (PPMS) (Quantum Design Inc., San Diego, CA, USA) equipped with a superconducting magnet with a maximum magnetic field of 140 kOe.

3. Results

3.1. Structural Properties

The TEM image in Figure 1a shows that the product synthesized at 433 K for six days consists of fan-shaped particles with a diameter size of about 500 nm, which were formed by an assembly of nanocones (Figure 1b). The microstructure at the edges of the fan-shaped particles shown in Figure 1b and an HADDF image in Figure 1c reveal a relatively flat surface of the fan-shaped particles assembled by two or three layers of nanocones. Such an intricate microstructure forms when the as-synthesized nanocones agglomerate, in order to minimize the magnetostatic energy [29]. The nanocones have different diameters at two ends, which gradually change from ~40 to ~5 nm and the length of the nanocones is about 200 nm (Figure 1d). A small amount of Fe₃O₄ nanocrystals with an average particle size of ~4 nm can be observed on the surface of the nanocones. The HRTEM image of a cubic nanocrystal (Figure 1e) shows a lattice fringe with spacing of approximately 0.26 nm, which represents the (311) planes (0.253 nm) of the cubic Fe₃O₄ according to the Joint Committee on Powder Diffraction Standards (JCPDS) XRD card (19–0629). The Fe₃O₄ nanocrystals should come from the oxidation of excess of Fe nanocrystals (NCs) without carbon coating. The HRTEM image in Figure 1f demonstrates a typical core-shell structure of an individual nanocone with the thickness of the carbon shell being about 2–3 nm. However, there is no evident lattice fringe spacing for the nanocone, indicating the poor crystallization or crystallite constituents with very small grain size.

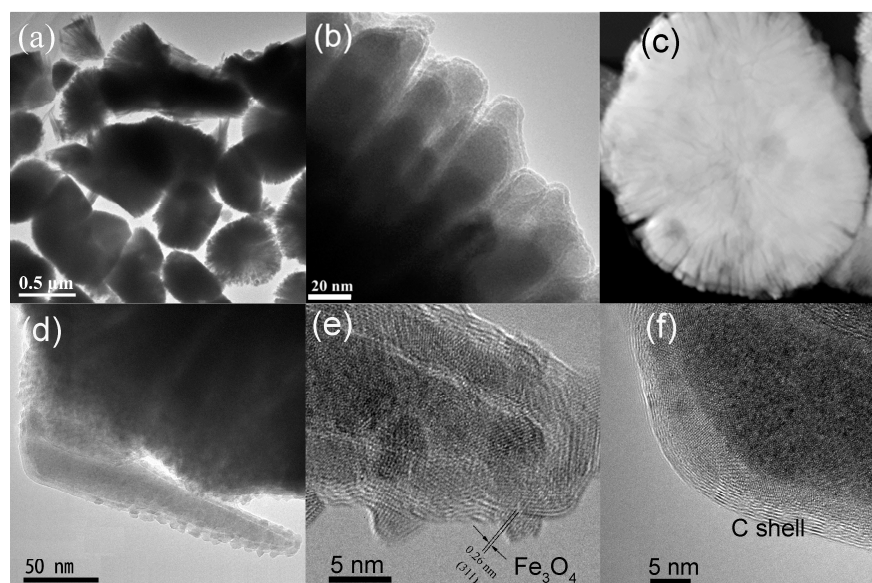


Figure 1. (a,b) TEM image and (c) HADDF images of α'' -Fe₁₆N₂@C nanocones synthesized at 433 K for six days. (d) TEM image for a separate α'' -Fe₁₆N₂@C nanocone and its corresponding HRTEM image for (e) Fe₃O₄ nanocrystals on the surface of the thinner end and (f) carbon shell of the thicker end.

Figure 2 shows the phase evolution of final products synthesized at the different reaction conditions, such as the reaction temperature and time. The powder XRD pattern in Figure 2a indicates that the sample synthesized at 393 K for three days consisted of Fe₃O₄ and α -Fe. The Fe₃O₄ and α -Fe NCs agglomerated into spherical particles under the magnetostatic energy (not shown here). When the nitridation reaction was performed at 403 K for three days, the powder XRD pattern of the as-prepared sample in Figure 2b reveals that the XRD peaks can be indexed to α -Fe with the JCPDS XRD card (06–696), α'' -Fe₁₆N₂ with the JCPDS XRD card (78–1865) and a small amount of Fe₃O₄ characterized by a weak (311) XRD peak at $2\theta = 35.4^\circ$. When the reaction temperature and time were increased to 433 K and six days, respectively, Figure 2c shows that the product consisted of the main phase α'' -Fe₁₆N₂ and a trace amount of Fe₃O₄. There is no α -Fe in the product due to the oxidation of excess of α -Fe NCs without carbon coating, as presented in Figure 1d,e. The XRD peaks of the as-synthesized α'' -Fe₁₆N₂ nanocones in Figure 2c match well with the standard XRD pattern of bulk α'' -Fe₁₆N₂ (JCPDS card no. 78–1865) that has a tetragonal structure with a space group of I4/mmm (139) and $a = b = 5.72 \text{ \AA}$, and $c = 6.29 \text{ \AA}$ (Figure 2e). The main peak position of the product with a nanocone shape is consistent with that of (202) for α'' -Fe₁₆N₂, indicating that the properly increased reaction temperature and time were helpful to the diffusion of N atoms into α -Fe nanocrystals for the formation of α'' -Fe₁₆N₂. However, the (202) XRD peak around $2\theta \approx 42.7^\circ$ and (220) XRD peak around $2\theta \approx 44.8^\circ$ for α'' -Fe₁₆N₂ emerge as a broad peak, revealing the poor crystallization or α'' -Fe₁₆N₂ crystallite with small grain sizes in the nanocones. The average grain size of α'' -Fe₁₆N₂ nanocrystals calculated by the Scherrer formula was about 3 nm, in good agreement with the HRTEM result shown in Figure 1d. After raising the reaction temperature and time to 453 K and six days (Figure 2d), the main peak position (2θ) of the product shifted from 42.7° for α'' -Fe₁₆N₂ to 43.05° and a new XRD peak at 41.3° emerged for the (111) of γ -Fe₄N (JCPDS card no. 06–627). This reveals that extra N atoms will transform the α'' -Fe₁₆N₂ to a stable phase of γ -Fe₄N. There was no carbon detected in the XRD patterns due to the slight amount. XPS was used to detect the species covering on the surface of the nanocones. Figure 3a represents the XPS spectra of the as-prepared and surface-cleaned α'' -Fe₁₆N₂ nanocones synthesized at 433 K for six days. The binding energies at 284.6 and 285.7 eV in the XPS spectra in Figure 3b reveal ordered and disordered carbon, respectively, on the surfaces of α'' -Fe₁₆N₂ nanocones, which is consistent with the Raman data shown as the

inset in Figure 3b. Figure 3c shows the XPS spectra of Fe2p. The binding energies of Fe2p_{3/2} at about 706.7 and 710.4 eV should be assigned to α'' -Fe₁₆N₂ and Fe₃O₄, respectively. The XPS peak area corresponding to Fe₃O₄ decreased significantly when we extended the Ar ion sputtering time from 0 s to 60 s, confirming the slight Fe₃O₄ existing on the surfaces of α'' -Fe₁₆N₂ nanocones. The weak binding energy peak at 397.3 eV featured by the blue line in Figure 3d was assigned to the N element in α'' -Fe₁₆N₂, while that at 399.0 eV featured by the red line was assigned to the C-N from TEPA adsorbed on the surface of the nanocones.

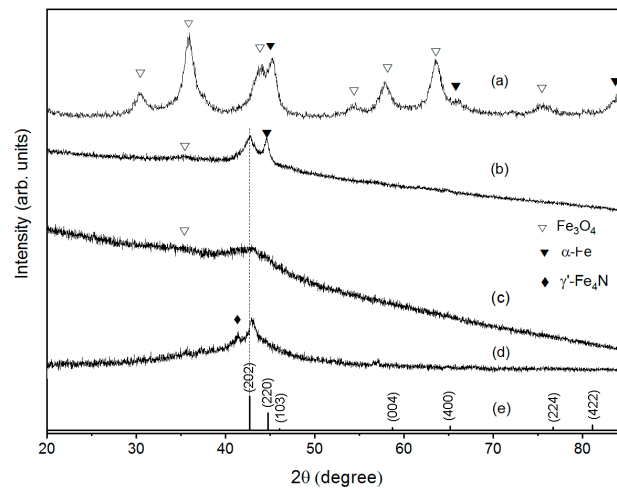


Figure 2. Powder XRD patterns of the products synthesized under different reaction conditions: (a) 393 K and three days, (b) 403 K and three days, (c) 433 K and six days, (d) 453 K and six days, (e) JCPDS XRD card of #78-1865 for α'' -Fe₁₆N₂.

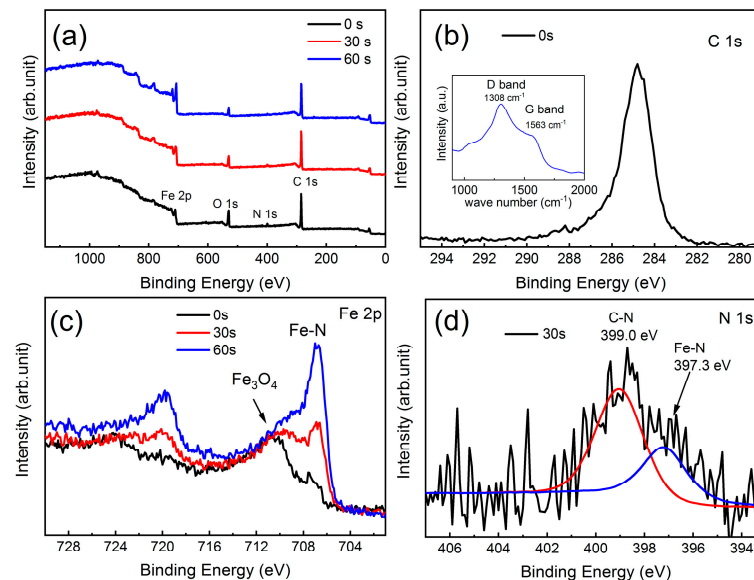
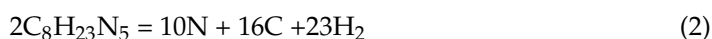


Figure 3. XPS spectra of the α'' -Fe₁₆N₂@C nanocones synthesized at 433 K for six days. (a) Survey of the sample with the surfaces cleaned for 0 s, 30 s and 60 s, respectively. (b) C 1s, (c) Fe 2p and (d) N 1s spectra. The inset in (b) shows the Raman spectrum of the as-prepared α'' -Fe₁₆N₂@C nanocones.

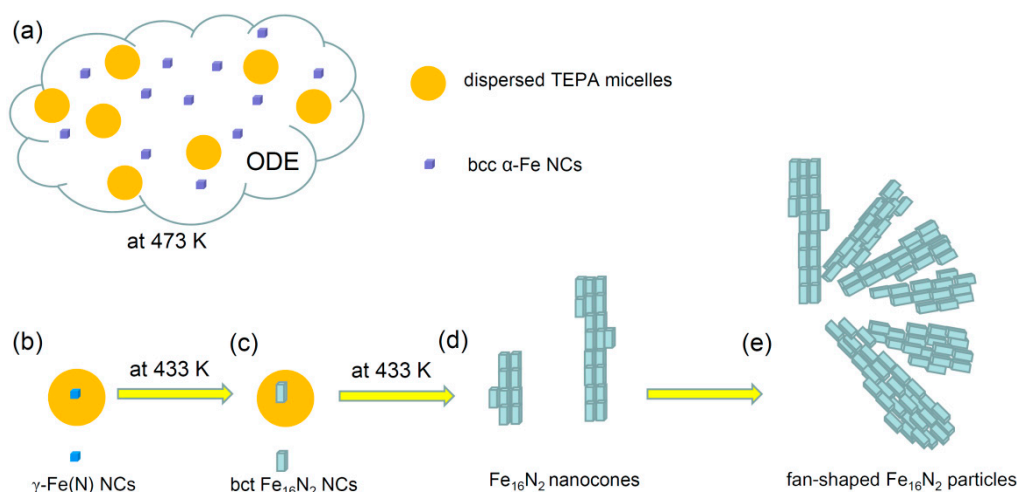
3.2. Anisotropic Growth

A previous study of the ϵ -Fe₃N_{1+x}@C nanoparticles revealed the nitridation and growth mechanism of core/shell structured ϵ -Fe₃N_{1+x}@C nanoparticles in a low-temperature wet chemical route [31]. In contrast to the nearly spherical shape of ϵ -Fe₃N_{1+x}@C nanoparticles, the anisotropic α'' -Fe₁₆N₂ nanocones may possess a different growth mechanism. Scheme 1 presents the anisotropic growth mechanism of the α'' -Fe₁₆N₂ nanocones in the ODE-TEPA

solution reaction system. Unlike a previous oil-in-water (o/w) microemulsion that was stable below 333 K [36], a stable TEPA-in-ODE (TEPA/ODE) microemulsion was formed by simply heating a mixture of TEPA, ODE and OLA at a temperature higher than 393 K. It should be noted that the OLA served as a surfactant for dispersing the α -Fe nanocrystals, which is not necessary for the formation of a stable TEPA/ODE microemulsion. When a mixed solution of 2 mL of $\text{Fe}(\text{CO})_5$, 6 mL of ODE and 2 mL of OLA in a syringe was injected into the TEPA/ODE microemulsion at 473 K, body-centered cubic (bcc) α -Fe nanocrystals (NCs) were first formed in the ODE phase by thermal decomposition of $\text{Fe}(\text{CO})_5$. Under magnetic stirring, the bcc α -Fe NCs were transferred into the TEPA micelles. Based on the reaction mechanism [31], the α -Fe NCs catalytically decomposed TEPA to form N and C atoms. It should be noted that the reaction rate for the formation of C and N atoms may have been slow due to a reaction temperature of 433 K, which is much lower than the reaction temperature of 533 K for the ϵ - $\text{Fe}_3\text{N}_{1+x}$ @C nanoparticles [31]. At the initial stage, a small amount of N atoms diffused into α -Fe NCs to form $\text{Fe}(\text{N})$ NCs. With increasing reaction time, more N atoms participated in the nitridation reaction and tetragonal α'' - Fe_{16}N_2 NCs would be formed. In the case of synthesis of ϵ - Fe_3N @C nanoparticles in TEPA, Fe NCs easily agglomerated to form nearly spherical nanoparticles with a wide particle size distribution of 100–500 nm in diameter [11]. However, in the present case, the interface between the nonpolar ODE phase and polar TEPA micelles controlled the Fe NCs transferring from the ODE phase to the TEPA phase. Once the tetragonal α'' - Fe_{16}N_2 NCs were formed in the TEPA micelles, the magnetic α'' - Fe_{16}N_2 NCs could assemble along the crystallographic *c* axis of α'' - Fe_{16}N_2 NCs to form α'' - Fe_{16}N_2 nanocones. Magnetocrystalline anisotropy energy is suggested as the driving force because the easy magnetization direction of tetragonal α'' - Fe_{16}N_2 NCs was along the *c* axis. With the reaction going on, more and more C atoms were left on the surfaces of α'' - Fe_{16}N_2 nanocones, resulting in a core/shell structure. The reaction would be cut off when the α'' - Fe_{16}N_2 nanocones were completely covered by the carbon shell. The overall reaction processes can be speculated as following the reaction Equations (1)–(4):



The catalytic decomposition of $\text{C}_8\text{H}_{23}\text{N}_5$ (TEPA) should occur on the surface of α -Fe NCs due to the large surface energy. Smaller α -Fe NCs allowed easier production and diffusion of N atoms into them for the synthesis of the iron nitride phase [31]. When the reaction was stopped by cooling the reaction temperature from 433 K to room temperature, the TEPA/ODE microemulsion broke and the reaction system separated into a TEPA layer and an ODE layer at about 393 K. Meanwhile, the α -Fe NCs left in the ODE phase were magnetically attracted to the thinner end of the α'' - Fe_{16}N_2 @C nanocones due to higher magnetic flux density than that on the thicker end (see Figure 1d). The formation of fan structures may have been driven by the reduction of high surface energy and/or by the magnetostatic energy. However, the thinner ends of the α'' - Fe_{16}N_2 nanocones directed the centers of the fan-shaped particles due to a higher magnetic flux density of the thinner end than the thicker end, indicating that magnetostatic energy was the dominant driving force in the formation of fan-shaped particles. The α -Fe NCs were oxidized to Fe_3O_4 , while α'' - Fe_{16}N_2 nanocones were protected by carbon shells from oxidation in an air atmosphere, in good agreement with the XPS and HRTEM results. As a result, anisotropic α'' - Fe_{16}N_2 @C nanocones with a core-shell structure were successfully synthesized in a new TEPA/ODE microemulsion system at a low temperature of 433 K and six days.



Scheme 1. Schematic illustration of the growth mechanism of fan-shaped $\alpha''\text{-Fe}_{16}\text{N}_2\text{@C}$ nanocones in a nonpolar–polar ODE-TEPA microemulsion system. (a) $\text{Fe}(\text{CO})_5$ decomposed in the ODE to form bcc $\alpha\text{-Fe}$ NCs. (b) Fe NCs migrated into TEPA micelles and N atoms produced by decomposition of TEPA, which diffused into bcc Fe NCs to form $\gamma\text{-Fe}(\text{N})$ NCs. (c) Formation of bcc $\alpha''\text{-Fe}_{16}\text{N}_2$ NCs. (d) $\alpha''\text{-Fe}_{16}\text{N}_2$ NCs assembled to $\alpha''\text{-Fe}_{16}\text{N}_2$ nanocones. The carbon shells formed on the surface of $\alpha''\text{-Fe}_{16}\text{N}_2$ were omitted for clarity. (e) $\alpha''\text{-Fe}_{16}\text{N}_2\text{@C}$ nanocones agglomerated to form fan-shaped particles due to the magnetostatic interaction.

3.3. Thermal Property

Thermal analyses of the $\alpha''\text{-Fe}_{16}\text{N}_2\text{@C}$ nanocones synthesized at 433 K for six days are shown in Figure 4. The TGA curve in Figure 4a exhibits two steps of weight (W) loss in a temperature between 310 K and 800 K. The first step is a slight weight loss (~ 1 wt.%) below an onset temperature ($T_{\text{onset}} = \sim 470$ K) due to the loss of organic molecules adsorbed on the surface of nanocones. The T_{onset} corresponds to an onset temperature for the decomposition of $\alpha''\text{-Fe}_{16}\text{N}_2$ due to high temperature. The second step covers a broad temperature range between T_{onset} and 800 K. The temperature dependence of dW/dT clearly displayed that the stage between 470 K and 600 K corresponded to release of the N atoms from $\alpha''\text{-Fe}_{16}\text{N}_2$, while the stage between 600 K and 800 K may have originated from the reduction of iron oxide by the carbon shells of $\alpha''\text{-Fe}_{16}\text{N}_2\text{@C}$ nanocones following a possible reaction of $\text{Fe}_3\text{O}_4 + 4\text{C} = 3\text{Fe} + 4\text{CO}$. As a result, the weight loss of ~ 8 wt.% in the second step should be ascribed to the losses of ~ 3 wt.% nitrogen atoms from $\alpha''\text{-Fe}_{16}\text{N}_2$ and ~ 5 wt.% oxygen/carbon atoms due to the losses of oxygen atoms and carbon atoms. Our previous work [37] indicates that amorphous iron oxides on the surfaces of $\epsilon\text{-Fe}_3\text{N}$ nanoparticles become Fe_3O_4 and Fe_2O_3 crystals at a temperature near 623 K, but loss of oxygen at a temperature between 623 and 793 K. This suggests that the $\alpha''\text{-Fe}_{16}\text{N}_2\text{@C}$ nanocones were metastable below ~ 470 K and the weight loss of ~ 3 wt.% from 470 to 600 K is in good agreement with the weight percentage of N atoms in $\alpha''\text{-Fe}_{16}\text{N}_2$. Besides the reactions for the decomposition of $\alpha''\text{-Fe}_{16}\text{N}_2$ and the redox reduction of Fe_3O_4 , an endothermic reaction also happened at about 600 K, as revealed by the DSC curve (Figure 4b). The possible reaction was $5\text{Fe}_{16}\text{N}_2 + 32\text{C} = 16\text{Fe}_5\text{C}_2 + 5\text{N}_2$. Compared with Figure 1b, the XRD pattern in Figure 5a reveals almost no change of the $\alpha''\text{-Fe}_{16}\text{N}_2\text{@C}$ nanocones heat-treated at 483 K. However, the main phase became Fe_5C_2 (JCPDS card no. 51-0529) when the $\alpha''\text{-Fe}_{16}\text{N}_2\text{@C}$ nanocones were heated to 600 K (Figure 5b). The main phase of Fe_5C_2 heated at 600 K proves the loss of N atoms from the $\alpha''\text{-Fe}_{16}\text{N}_2\text{@C}$ nanocones at a temperature lower than 600 K.

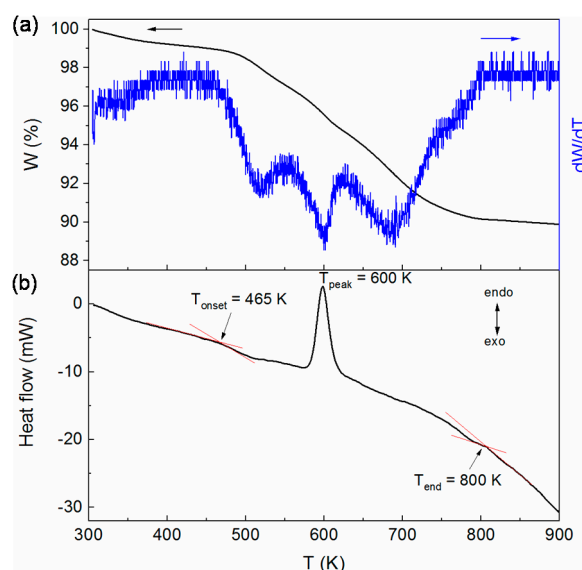


Figure 4. (a) TGA and dW/dT curves, (b) DSC curve of the α'' - Fe_{16}N_2 @C nanocones recorded in the heating process in a temperature range between 300 and 900 K.

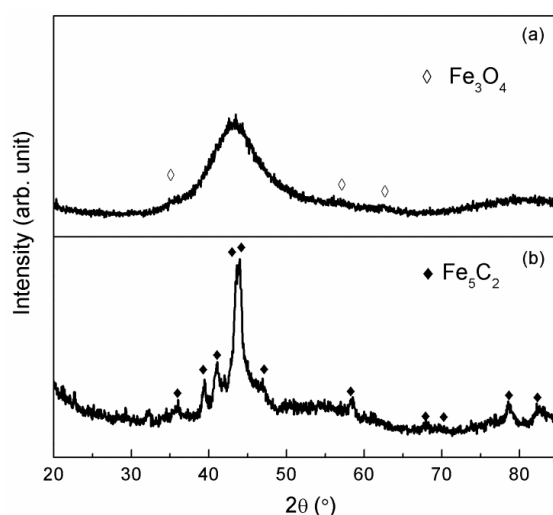


Figure 5. XRD patterns of the products heated at (a) 483 K and (b) 600 K in a vacuum.

3.4. Magnetic Properties

Figure 6a represents the room-temperature magnetic hysteresis loops of the α'' - Fe_{16}N_2 @C nanocones synthesized at 433 K for six days and at 413 K for six days, respectively, with characteristics of ferromagnetic materials. The saturation magnetization (M_S) and the coercivity (H_C) were respectively 83 emu/g and 320 Oe at 300 K for the α'' - Fe_{16}N_2 @C nanocones synthesized at 433 K for six days, while the M_S and the H_C became 81.6 emu/g and 250 Oe at 300 K for the α'' - Fe_{16}N_2 @C nanocones synthesized at 413 K for six days. The decrease in the magnetic properties of the α'' - Fe_{16}N_2 @C nanocones may be ascribed to a slight composition change of α'' - Fe_{16}N_2 due to the reduced reaction temperature. Nevertheless, the saturation magnetizations were much lower than the previously reported M_S (290 emu/g) for α'' - Fe_{16}N_2 thin film [9]. According to our previous work on the carbon-coated ϵ - $\text{Fe}_3\text{N}_{0.88}$ nanoparticles, the carbon shells reduce the M_S of ϵ - $\text{Fe}_3\text{N}_{0.88}$ nanoparticles by a value of 11.8% [11]. Thus, the M_S value of the α'' - Fe_{16}N_2 nanocones would slightly increase if removing the negative effect of diamagnetic carbon. Considering the XRD pattern in Figure 2c, the fraction of Fe_3O_4 nanoparticles was very small and can be neglected, while the minimum fraction of carbon was ~ 8 wt.% estimated based on the Fe_5C_2 phase in Figure 5b. Taking the diamagnetic susceptibility of about -1.4×10^{-5} emu/g \cdot Oe

at 300 K for carbon [38], the M_S of α'' -Fe₁₆N₂ nanocones increased at least to 90.24 emu/g at 300 K by removing the C shells from the α'' -Fe₁₆N₂@C nanocones. Figure 6b plots the temperature dependence of magnetization (M - T) of the α'' -Fe₁₆N₂@C nanocones in the warming and the cooling processes in a temperature range between 300 and 900 K. The M - T curves in the warming and the cooling processes were irreversible. The M - T curve in the warming process A shows a decrease of magnetization with an increasing temperature with a knee point at about 510 K. It reveals the thermal decomposition of α'' -Fe₁₆N₂, which was a little higher than the temperature determined by thermal analysis (Figure 4). Below the thermal decomposition temperature of 510 K, the α'' -Fe₁₆N₂ was metastable (Figure 5a). Above 600 K, the magnetization in the warming process became almost a constant. The M - T curve recorded in the cooling process B (Figure 6b) presents a magnetic transition temperature at 528 K, which was determined by the point of intersection of the two tangents around the inflection point of the cooling M - T curve. The ferromagnetic–paramagnetic transition at 528 K should be ascribed to the Fe₅C₂ phase determined by the XRD pattern (Figure 5b). Such a T_C of 528 K for Fe₅C₂ agrees with the T_C value previously reported for Fe₅C₂ [39]. There were no magnetic transitions in the cooling process B between 550 and 600 K and in the warming process A between 600 and 900 K. The absence of magnetic phases of ϵ -Fe₃N ($T_C = 575$ K), γ -Fe₄N ($T_C = 760$ K) and Fe₃O₄ ($T_C = 864$ K) reveals that all the N atoms had been released from the α'' -Fe₁₆N₂ nanocones and Fe₃O₄ had been reduced by carbon in the warming process A. Figure 4a suggests that the reduction of Fe₃O₄ by carbon happened at a temperature range of 600–800 K, revealing a mass loss about 5 wt.% due to the loss of oxygen. The magnetic product of Fe₃O₄ reduced by carbon is α -Fe. The M - T curve recorded in the cooling process C (Figure 6b) shows two different magnetic transitions at 483 and above 900 K, respectively. The magnetic transition temperature of 483 K is in good agreement with the T_C of Fe₃C, while the magnetic transition above 900 K may be ascribed to α -Fe. However, the change of the magnetization after raising the temperature from 700 to 900 K in process C was not obvious due to a small amount of α -Fe and a higher magnetic transition temperature of α -Fe ($T_C \approx 1043$ K). It is reasonable that the magnetizations in the process B at the temperature range of 500–600 K (Figure 6b) were smaller than those in the process A due to existence of α'' -Fe₁₆N₂ and in process C due to existence of a small amount of Fe. It is possible that the α -Fe partially diffused into the Fe₅C₂ to form Fe₃C following the reaction equation of Fe₅C₂ + Fe = 2Fe₃C, but leaving a small amount of α -Fe in the product heated up to 900 K.

Despite the low saturation magnetization and coercivity at room temperature, anisotropic 1D α'' -Fe₁₆N₂@C nanocones were synthesized for the first time in a one-pot chemical solution method. It has been found that diamagnetic carbon shells weaken the saturation magnetization of α'' -Fe₁₆N₂ nanocones although the carbon shells can protect the α'' -Fe₁₆N₂@C nanocones from oxidation in an air atmosphere. The Fe NCs with small particle sizes were easily nitridized to form α'' -Fe₁₆N₂, but small grain sizes of α'' -Fe₁₆N₂ NCs may be detrimental to their high coercivity performance. The theoretical shape anisotropy field was $2\pi M_S$ for the nanowire with very high aspect ratio. Moreover, in nanowire arrays, the dipolar interaction between wires becomes important. The maximum field originating from dipole–dipole interactions was $-2\pi PM_S$ when the magnetization was saturated perpendicular to the wire axis, and $4\pi PM_S$ when the magnetization was saturated along the wire axis, where P was a packing density of the nanowire array [40]. The low coercivity at room temperature for the present anisotropic 1D α'' -Fe₁₆N₂@C nanocones may have resulted from the fan-like agglomerated structure, which can form a magnetic vortex different from the magnetic state produced by separate elongated particles. Therefore, to enhance the hard magnetic properties of the α'' -Fe₁₆N₂@C nanocones, it is worth studying the syntheses of α'' -Fe₁₆N₂ nanocones/nanorods with controllable grain/particle sizes and alignments of the separate 1D nanorods/nanocones instead of a fan-like structure. Moreover, as has been demonstrated in the ϵ -Fe₃N_{1+x} ($x \leq 0$) [11], finely engineering the N content in the iron nitride nanostructures and removing the impurity are also critical to increase the saturation magnetization of α'' -Fe₁₆N₂@C material. Our low-temperature

chemical synthesis for 1D α'' -Fe₁₆N₂ nanostructures has potential to obtain high permanent magnetic performance. Efforts to synthesis a magnetically oriented 1D α'' -Fe₁₆N₂ hard magnet are still in progress.

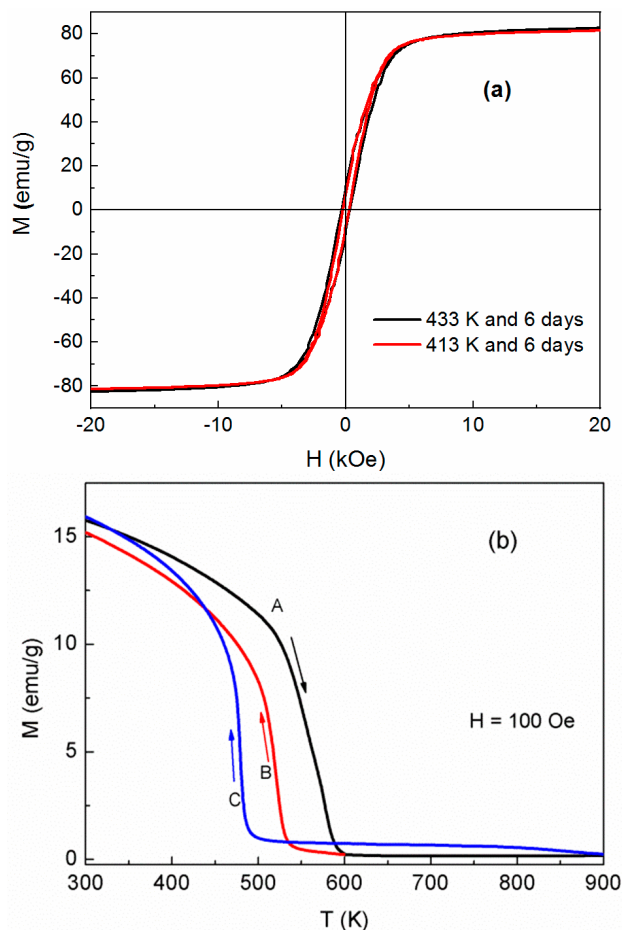


Figure 6. (a) Magnetic hysteresis loops of the α'' -Fe₁₆N₂@C nanocones synthesized at 433 K for six days and at 413 K for six days, respectively. (b) Temperature dependence of magnetization of the α'' -Fe₁₆N₂@C nanocones synthesized at 433 K and six days in (A) a warming process between 300 and 900 K and the cooling processes from different temperature of (B) 600 K and (C) 900 K, respectively, to 300 K.

4. Conclusions

We developed a facile protocol for synthesizing carbon-coated tetragonal α'' -Fe₁₆N₂ nanocones by a new one-pot microemulsion method with Fe(CO)₅ serving as the iron source and TEPA as the N/C source. Anisotropic growth of the tetragonal α'' -Fe₁₆N₂@C nanocones is ascribed to the strong magnetocrystalline anisotropy energy of α'' -Fe₁₆N₂ nanocrystals. α'' -Fe₁₆N₂@C nanocones agglomerated to form a fan-shaped microstructure due to the magnetostatic energy. 1D α'' -Fe₁₆N₂@C nanocones have excellent oxidation resistance. Despite their hard magnetic characteristics with room-temperature saturation magnetization and coercivity of 82.6 emu/g and 320 Oe, respectively, the energy produced is low due to the low saturation magnetization and coercivity of the material. However, as has been demonstrated, the magnetic properties are easily tunable by the content of ordering N atoms and grain sizes. Systematic experimental work is under way to enhance the saturation magnetization and coercivity of 1D α'' -Fe₁₆N₂@C nanocones. If these properties are enhanced, 1D α'' -Fe₁₆N₂ aligned hard-magnetic materials can be a low-cost, nontoxic alternative to noble-metal- or rare-earth-element-based advanced magnets.

Author Contributions: Conceptualization, D.L. and Y.L.; methodology, D.L.; investigation, Y.L., Q.K. and X.M.; formal analysis, Y.L., Q.K. and S.W.; resources, D.L. and Z.Z.; data curation, Y.L.; writing—original draft preparation, D.L. and Y.L.; writing—review and editing, D.L., C.C. and Z.Z.; supervision, D.L. and Z.Z. All authors have read and agreed to the published version of the manuscript.

Funding: This research was funded by Future Materials Discovery Program through the National Research Foundation of Korea (NRF) funded by the Ministry of Science and Technology and ICT (2016M3D1A1027835), by the National Natural Science Foundation of China under Grant No. 51971221, 52031014 and by the National Key R&D Program of China (No. 2017YFA0206302, No. 2017YFA0700702) from the ministry of Science and Technology of China.

Data Availability Statement: The data is available on reasonable request from the corresponding author.

Conflicts of Interest: There is no conflict to declare.

References

1. Coey, J.M.D. Hard Magnetic Materials: A Perspective. *IEEE Trans. Magn.* **2011**, *47*, 4671–4681. [\[CrossRef\]](#)
2. Li, D.; Pan, D.S.; Li, S.J.; Zhang, Z.D. Recent developments of rare-earth-free hard-magnetic materials. *Sci. China Phys. Mech. Astron.* **2016**, *59*, 617501. [\[CrossRef\]](#)
3. Li, D.; Li, Y.; Pan, D.S.; Zhang, Z.D.; Choi, C.J. Prospect and status of iron-based rare-earth-free permanent magnetic materials. *J. Magn. Magn. Mater.* **2019**, *469*, 535–544. [\[CrossRef\]](#)
4. Gao, C.; Doyle, W.D.; Shamsuzzoha, M. Quantitative Correlation of phase-structure with the magnetic-moments in rf-sputtered Fe-N Films. *J. Appl. Phys.* **1993**, *73*, 6579–6581. [\[CrossRef\]](#)
5. Komuro, M.; Kozono, Y.; Hanazono, M.; Sugita, Y. Epitaxial-growth and magnetic-properties of Fe₁₆N₂ films with high saturation magnetic-flux density. *J. Appl. Phys.* **1990**, *67*, 5126–5130. [\[CrossRef\]](#)
6. Okamoto, S.; Kitakami, O.; Shimada, Y. Alpha"-Fe₁₆N₂ phase epitaxially grown by sputter beam method. *J. Appl. Phys.* **1996**, *79*, 5250–5252. [\[CrossRef\]](#)
7. Nakajima, K.; Yamashita, T.; Takata, M.; Okamoto, S. Mössbauer study on Fe₁₆N₂ films prepared by ion-implant nitrification of iron films. *J. Appl. Phys.* **1991**, *70*, 6033–6035. [\[CrossRef\]](#)
8. Takahashi, H.; Mitsuoka, K.; Komuro, M.; Sugita, Y. Ferromagnetic-resonance studies of Fe₁₆N₂ films with a giant magnetic-moment. *J. Appl. Phys.* **1993**, *73*, 6060–6062. [\[CrossRef\]](#)
9. Kim, T.K.; Takahashi, M. New magnetic material having ultrahigh magnetic moment. *Appl. Phys. Lett.* **1972**, *20*, 492–494. [\[CrossRef\]](#)
10. Coey, J.M.D.; Smith, P.A.I. Magnetic nitrides. *J. Magn. Magn. Mater.* **1999**, *200*, 405–424. [\[CrossRef\]](#)
11. Li, Y.; Pan, D.S.; Zhou, Y.T.; Kuang, Q.F.; Wang, C.W.; Li, B.; Zhang, B.S.; Park, J.; Li, D.; Choi, C.; et al. Enhanced magnetic properties and thermal stability of highly ordered ε-Fe₃N_{1+x} (−0.12 ≤ x ≤ −0.01) nanoparticles. *Nanoscale* **2020**, *12*, 10834–10841. [\[CrossRef\]](#) [\[PubMed\]](#)
12. Ishida, S.; Kitawatase, K. Electronic-structures and magnetic-properties of iron nitrides. *J. Magn. Magn. Mater.* **1992**, *104*, 1933–1934. [\[CrossRef\]](#)
13. Ji, N.A.; Allard, L.F.; Lara-Curzio, E.; Wang, J.P. N site ordering effect on partially ordered Fe₁₆N₂. *Appl. Phys. Lett.* **2011**, *98*, 092506. [\[CrossRef\]](#)
14. Jiang, Y.F.; Dabade, V.; Allard, L.F.; Lara-Curzio, E.; James, R.; Wang, J.P. Synthesis of α"-Fe₁₆N₂ compound anisotropic magnet by the strained-wire method. *Phys. Rev. Appl.* **2016**, *6*, 10.
15. Gandha, K.; Elkins, K.; Poudyal, N.; Liu, X.B.; Liu, J.P. High energy product developed from cobalt nanowires. *Sci. Rep.* **2014**, *4*, 5345. [\[CrossRef\]](#) [\[PubMed\]](#)
16. Zhang, H.W.; Long, G.; Li, D.; Sabirianov, R.; Zeng, H. Fe₃Se₄ nanostructures with giant coercivity synthesized by solution chemistry. *Chem. Mater.* **2011**, *23*, 3769–3774. [\[CrossRef\]](#)
17. Wang, C.; Hou, Y.L.; Kim, J.M.; Sun, S.H. A general strategy for synthesizing FePt nanowires and nanorods. *Angew. Chem. Int. Ed.* **2007**, *46*, 6333–6335. [\[CrossRef\]](#) [\[PubMed\]](#)
18. Jiang, Y.F.; Liu, J.M.; Suri, P.K.; Kennedy, G.; Thadhani, N.N.; Flannigan, D.J.; Wang, J.P. Preparation of an α"-Fe₁₆N₂ magnet via a ball milling and shock compaction approach. *Adv. Eng. Mater.* **2016**, *18*, 1009–1016. [\[CrossRef\]](#)
19. Kita, E.; Shibata, K.; Yanagihara, H.; Sasaki, Y.; Kishimoto, M. Magnetic properties of core-shell type Fe₁₆N₂ nanoparticles. *J. Magn. Magn. Mater.* **2007**, *310*, 2411–2413. [\[CrossRef\]](#)
20. Zuhijah, R.; Nandiyanto, A.B.D.; Ogi, T.; Iwaki, T.; Nakamura, K.; Okuyama, K. Gas phase preparation of spherical core-shell α"-Fe₁₆N₂/SiO₂ magnetic nanoparticles. *Nanoscale* **2014**, *6*, 6487–6491. [\[CrossRef\]](#)
21. Bridges, C.A.; Rios, O.; Allard, L.F.; Meyer, H.M.; Huq, A.; Jiang, Y.; Wang, J.P.; Brady, M.P. The impact of carbon coating on the synthesis and properties of α"-Fe₁₆N₂ powders. *Phys. Chem. Chem. Phys.* **2016**, *18*, 13010–13017. [\[CrossRef\]](#)
22. Ogi, T.; Nandiyanto, A.B.D.; Kisakibaru, Y.; Iwaki, T.; Nakamura, K.; Okuyama, K. Facile synthesis of single-phase spherical α"-Fe₁₆N₂/Al₂O₃ core-shell nanoparticles via a gas-phase method. *J. Appl. Phys.* **2013**, *113*, 164301. [\[CrossRef\]](#)

23. Ogawa, T.; Ogata, Y.; Gallage, R.; Kobayashi, N.; Hayashi, N.; Kusano, Y.; Yamamoto, S.; Kohara, K.; Doi, M.; Takano, M.; et al. Challenge to the synthesis of α'' -Fe₁₆N₂ compound nanoparticle with high saturation magnetization for rare earth free new permanent magnetic material. *Appl. Phys. Express* **2013**, *6*, 073007. [[CrossRef](#)]
24. Kikkawa, S.; Yamada, A.; Masubuchi, Y.; Takeda, T. Fine Fe₁₆N₂ powder prepared by low-temperature nitridation. *Mater. Res. Bull.* **2008**, *43*, 3352–3357. [[CrossRef](#)]
25. Li, D.; Li, S.J.; Zhou, Y.T.; Bai, Y.; Zhu, Y.L.; Ren, W.J.; Long, G.; Zeng, H.; Zhang, Z.D. Magnetization reversal and coercivity of Fe₃Se₄ nanowire arrays. *J. Appl. Phys.* **2015**, *117*, 17E702. [[CrossRef](#)]
26. Robbins, M.; White, J.G. Magnetic properties of ϵ -ion nitride. *J. Phys. Chem. Solids* **1964**, *25*, 717–720. [[CrossRef](#)]
27. Chen, G.M.; Jaggi, N.K.; Butt, J.B.; Yeh, E.B.; Schwartz, L.H. Mossbauer and magnetic studies of ϵ -Fe_xN, 2 < x < 3. *J. Phys. Chem.* **1983**, *87*, 5326–5332.
28. Jack, K.H. Binary and ternary interstitial alloys. 1. The iron-nitrogen system- the structure of Fe₄N and Fe₂N. *Proc. R. Soc. Lond. Ser. Math. Phys. Sci.* **1948**, *195*, 34–40.
29. Li, D.; Choi, C.J.; Kim, B.K.; Zhang, Z.D. Characterization of Fe/N nanoparticles synthesized by the chemical vapor condensation process. *J. Magn. Magn. Mater.* **2004**, *277*, 64–70. [[CrossRef](#)]
30. Yu, Y.S.; Mukherjee, P.; Tian, Y.; Li, X.Z.; Shield, J.E.; Sellmyer, D.J. Direct chemical synthesis of L1₀-FePtAu nanoparticles with high coercivity. *Nanoscale* **2014**, *6*, 12050–12055. [[CrossRef](#)] [[PubMed](#)]
31. Li, Y.; Pan, D.; Li, D.; Feng, Y.; Choi, C.J.; Liu, W.; Zhang, Z. Catalytic synthesis and enhanced Curie temperature of ϵ -Fe₃N@C nanostructure synthesized in a tetraethylenepentamine solution. *J. Magn. Magn. Mater.* **2018**, *465*, 736–742. [[CrossRef](#)]
32. Bhattacharyya, S. Iron Nitride Family at Reduced Dimensions: A Review of Their Synthesis Protocols and Structural and Magnetic Properties. *J. Phys. Chem. C* **2015**, *119*, 1601–1622. [[CrossRef](#)]
33. Kikkawa, S.; Kubota, K.; Takeda, T. Particle size dependence in low temperature nitridation reaction for Fe₁₆N₂. *J. Alloy. Compd.* **2008**, *449*, 7–10. [[CrossRef](#)]
34. Dirba, I.; Schwobel, C.A.; Diop, L.V.B.; Duerrschnebel, M.; Molina-Luna, L.; Hofmann, K.; Komissinskiy, P.; Kleebe, H.J.; Gutfleisch, O. Synthesis, morphology, thermal stability and magnetic properties of α'' -Fe₁₆N₂ nanoparticles obtained by hydrogen reduction of γ -Fe₂O₃ and subsequent nitrogenation. *Acta Mater.* **2017**, *123*, 214–222. [[CrossRef](#)]
35. Kartikowati, C.W.; Suhendi, A.; Zulhijah, R.; Ogi, T.; Iwaki, T.; Okuyama, K. Effect of magnetic field strength on the alignment of α'' -Fe₁₆N₂ nanoparticle films. *Nanoscale* **2016**, *8*, 2648–2655. [[CrossRef](#)] [[PubMed](#)]
36. Li, D.; Li, S.J.; Zhang, Y.; Jiang, J.J.; Gong, W.J.; Wang, J.H.; Zhang, Z.D. Monodisperse water-soluble γ -Fe₂O₃/polyvinylpyrrolidone nanoparticles for a magnetic resonance imaging contrast agent. *Mater. Res. Innov.* **2015**, *19*, S358–S362. [[CrossRef](#)]
37. Li, D.; Choi, C.J.; Yu, J.H.; Kim, B.K.; Zhang, Z.D. Nanocrystalline α -Fe and ϵ -Fe₃N particles prepared by chemical vapor condensation process. *J. Magn. Magn. Mater.* **2004**, *283*, 8–15. [[CrossRef](#)]
38. Li, D.; Han, Z.; Wu, B.; Geng, D.; Zhang, Z. Ferromagnetic and spin-glass behaviour of nanosized oriented pyrolytic graphite in Pb-C nanocomposites. *J. Phys. D Appl. Phys.* **2008**, *41*, 115005. [[CrossRef](#)]
39. Yang, C.; Zhao, H.B.; Hou, Y.L.; Ma, D. Fe₅C₂ Nanoparticles: A facile bromide-induced synthesis and as an active phase for fischer-tropsch synthesis. *J. Am. Chem. Soc.* **2012**, *134*, 15814–15821. [[CrossRef](#)] [[PubMed](#)]
40. Strijkers, G.J.; Dalderop, J.H.J.; Broeksteeg, M.A.A.; Swagten, H.J.M.; de Jonge, W.J.M. Structure and magnetization of arrays of electrodeposited Co wires in anodic alumina. *J. Appl. Phys.* **1999**, *86*, 5141–5145. [[CrossRef](#)]